Available online at www.sciencedirect.com
ScienceDirect
Applied Surface Science 254 (2008) 1636–1643
applied surface science
www.elsevier.com/locate/apsusc

Microstructure and mechanical properties of Al_2O_3–Al composite coatings deposited by plasma spraying

Zhijian Yin [a,b], Shunyan Tao [a,*], Xiaming Zhou [a], Chuanxian Ding [a]

[a] *The Key Laboratory of Inorganic Coating Materials, Shanghai Institute of Ceramics, Chinese Academy of Sciences, Shanghai 200050, PR China*
[b] *Graduate School of the Chinese Academy of Sciences, Beijing 100039, PR China*

Received 19 November 2006; received in revised form 30 April 2007; accepted 11 July 2007
Available online 20 July 2007

Abstract

Al_2O_3 and Al_2O_3–Al composite coatings were prepared by plasma spraying. Phase composition of powders and as-sprayed coatings was determined by X-ray diffraction (XRD), while optical microscopy (OM) and scanning electron microscopy (SEM) were employed to investigate the morphology of impacted droplets, polished and fractured surface, and the element distribution in terms of wavelength-dispersive spectrometer (WDS). Mechanical properties including microhardness, adhesion and bending strength, fracture toughness and sliding wear rate were evaluated. The results indicated that the addition of Al into Al_2O_3 was beneficial to decrease the splashing of impinging droplets and to increase the deposition efficiency. The Al_2O_3–Al composite coating exhibited homogeneously dispersed pores and the co-sprayed Al particles were considered to be distributed in the splat boundary. Compared with Al_2O_3 coating, the composite coating showed slightly lower hardness, whereas the coexistence of metal Al phase and Al_2O_3 ceramic phase effectively improved the toughness, strength and wear resistance of coatings.

Keywords: Plasma spraying; Al_2O_3–Al composite; Microstructure; Mechanical properties

1. Introduction

Thermal spraying process has been used successfully to produce a range of protective coatings for wear, erosion and heat resistance, as well as restoration of worn parts [1–3]. Especially, oxide ceramics such as Al_2O_3 ceramic coatings, having superior hardness, chemical stability and refractory character, are commonly utilized to resist wear by friction and solid particle erosion [4,5]. As a surface modification technique, atmospheric plasma spraying (APS) has been well-established to deposit various coatings [1,6]. However, plasma-sprayed coatings built up from the successively immediate solidification of the liquid or partially melted droplets onto target substrate typically present weak interface between splats and irregular reticula of microcracks and pores running through it [3,7]. The porosity and weak interface adversely affect the wear property and the cracks allow corrosive substance in the environment to attach the protective coating. In addition, these ceramic coatings are also vulnerable to thermal fatigue and delamination under mechanical load for its intrinsic brittleness. So, the application of plasma-sprayed Al_2O_3 coating are restricted in many industrial fields such as wear and erosion resistance, especially under increasingly severe conditions by the combination of intrinsic brittleness and microstructural defects [4,8]. In recent years, numerous studies have been conducted to improve the microstructure and resulting performance of plasma-sprayed ceramic coatings by incorporating metallic second phases into ceramic matrices [9,10]. Dong et al. [9] reported that the composite coatings prepared by plasma spraying Fe_2O_3–Al self-reaction composite powders possessed multiphase metal and ceramic coexistence, which significantly decreased the brittleness and increased the wear resistance of coatings even when the load was up to 490 N. In Chwa et al.'s [10] study, plasma-sprayed nanostructured TiO_2–Al composite coatings were prepared, and the results obtained from experimental work showed that the Al addition effectively improved the deposition efficiency and mechanical properties of coatings including toughness and wear resistance.

In this work, aluminum, having excellent ductility and thermal conductivity, was added to prepare Al_2O_3–Al

* Corresponding author. Tel.: +86 21 52414101; fax: +86 21 52413903.
E-mail address: shunyantao@mail.sic.ac.cn (S. Tao).

0169-4332/$ – see front matter © 2007 Elsevier B.V. All rights reserved.
doi:10.1016/j.apsusc.2007.07.135

composite coating. The present study is related to detailed characterization of microstructure of Al_2O_3 and Al_2O_3–Al composite coatings deposited by plasma spraying, and to understand the effect of Al additive on the microstructure, mechanical properties and the tribological behaviors of coatings under different degree of severity using block-on-ring configuration.

2. Experimental details

2.1. Spray powder preparation

The commercially available Al_2O_3 powders with an average particle size of 33.5 μm were used as a feedstock in the present study. The raw feedstock has the purity >99.0 wt.% of Al_2O_3 component. And also, fine aluminum powders with an average particle size of 1–2 μm were used as an additive to prepare the other feedstock of Al_2O_3–Al composite. The composite powders with a content of around 5% Al were directly mechanically mixed in a rotary-vibration mill, polyvinyl alcohol being used as a binder, and then suffered sieving and drying prior to the spraying. The concept of spraying Al_2O_3–Al composite powder design in this study is schematically shown in Fig. 1.

2.2. Plasma spraying

The Metco A-2000 atmospheric plasma spraying equipment with F4-MB plasma gun (Sulzer Metco AG, Switzerland) was applied to prepare Al_2O_3 and Al_2O_3–Al composite coatings. The feedstock powders were fed with a Twin-System 10-C (Plasma-Technick AG, Switzerland). A mixture of argon and hydrogen was used as plasma gas. During spraying, the substrates and coatings were cooled using compressed air. Stainless steel coupons with dimension of approximately 50 mm × 20 mm × 2 mm were used as substrates. Before spraying, the substrates were degreased ultrasonically in acetone and grit blasted with corundum. In addition, the plasma torch was utilized to spray powders onto the unheated quartz substrate in order to observe the spreading and flattening morphology of impacted droplets. The details of operating spraying parameters are listed in Table 1.

2.3. Characterization

The phase composition of the powders and as-sprayed coatings was analyzed using XRD with nickel filtered Cu Kα

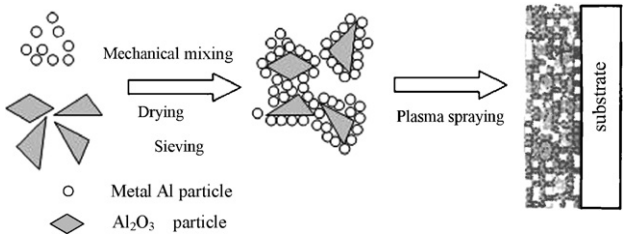

Fig. 1. The schematic diagram showing the concept of spraying powder design of Al_2O_3–Al composite.

Table 1
Plasma spraying parameters for Al_2O_3 and Al_2O_3–Al composite powders

Parameters	Unit	Value
Arc current	A	660
Primary gas (Ar) flow rate	slpm	49
Secondary gas (H_2) flow rate	slpm	12
Spray distance	mm	110
Carrier gas (Ar) flow rate	slpm	3.5
Injection diameter	mm	1.8

(λ = 1.54056) radiation on a Rigaku D/Max2550 Diffractometer. The microstructure of powders and coatings was determined employing an EMPA-8705 QH_2 electron probe analyzer (Shimadzu, Tokyo, Japan) with affiliated wavelength-dispersive spectrometer (WDS) detector. The morphology of individual and multiple impinged droplets collected on unheated quartz substrates was observed using optical microscopy (Instron, 2100B).

Porosity of coatings was estimated by quantitative image analysis. Ten fields are selected for the measurement of porosity [11]. Vickers microhardness measurements were conducted on the polished cross-section of coatings using a HX-1000 Microhardness Tester under a load of 200 g with a dwell time of 15 s. The coatings hardness values represent the average of 20 single measurements. The toughness of the coatings was calculated by measuring the crack length originating from the corners of the Vickers indentation (Instron 2100B) with a load of 5 kg applied for 10 s [12–14]. To avoid the effect of stress field, the distance between nearby indentations was kept longer than three times of the indentation diagonal for microhardness and toughness measurement [15]. Although not providing the absolute value of fracture toughness like that measured by the tapered double cantilever beam (TDCB) approach [16,17], the results obtained using this indentation technique can provide a sound relative comparison of the fracture toughness of various coatings [13,18].

Preliminary three-point bending tests (Instron 5566) of the free-standing coatings specimens (3 mm × 4 mm × 36 mm) were done with a cross-head speed of 0.5 mm/min and a span length of 20 mm to obtain the bending strength. To obtain the free-standing samples used in this study, coatings of 5 mm thickness were deposited onto the aluminium substrate and, then, were removed from the substrate. During spraying, the backs of substrates were cooled using circulating water, while the coating surfaces were cooled by compressed air. Adhesion strength of coatings was evaluated by tensile adhesion tests (Instron 5592) according to ASTM C 633-79. Five measurements were performed to determine the average bending and tensile adhesion strength for each coating.

The friction and wear behavior of coatings against stainless steel were evaluated under different degrees of severity using block-on ring arrangement. The dimensions of block and ring are 30 mm × 7 mm × 6 mm and $\Phi_{outer}40 \times \Phi_{inner}16 \times 10$ mm. The thickness and surface roughness of coatings, applied onto stainless steel ring, were around 320 and 0.2 μm after polishing, respectively. Prior to testing, the samples were cleaned in an ultrasonic bath with acetone for 15 min. When considering the

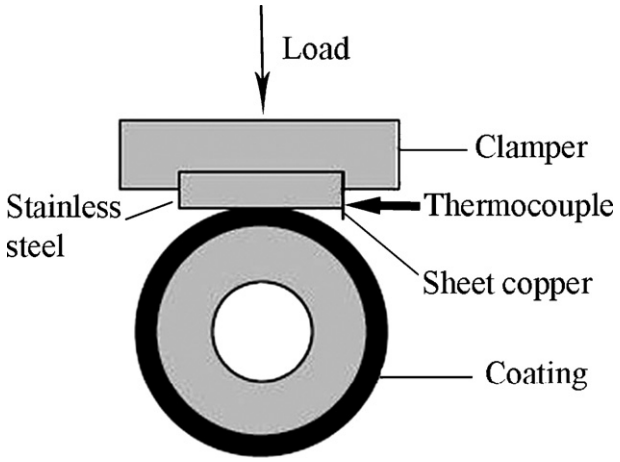

Fig. 2. Schematic diagram of the block-on-ring tester equipped with a thermal couple.

scatter of data, the friction coefficients and wear rate were the average of three identical samples. During the frictional testing, a thermocouple, as indicated in Fig. 2 by schematic diagram, was employed to measure friction temperature, which can be used to perform a sound comparison of the tribological heat generated and concentrated on the contact area of friction pairs under different conditions.

3. Results and discussions

3.1. Characterization of spraying powders

Fig. 3 shows the morphologies of the as-received feedstock powders. It can be seen that the Al_2O_3 particles, showing an irregular and angular morphology, were nearly enwrapped well by fine Al particles, which is confirmed by the internal morphology of Al_2O_3–Al composite powders, as shown in Fig. 4. And also, the result of particle size distribution, as indicated in Fig. 5 by a laser scatter particle size analyzer, shows no significant difference in these two feedstock powders.

Fig. 6 presents the XRD patterns of the powders and as-sprayed Al_2O_3 and Al_2O_3–Al composite coatings. It is found that the original powders are nearly all α-Al_2O_3. However, the coatings consist of γ-Al_2O_3 phase coexisting with some α-Al_2O_3 phase. It is suggested that the preferential formation of γ-Al_2O_3 is attributed to the high cooling rate (about 10^6 K/s) of the molten particles during plasma spraying and easy nucleation of γ-Al_2O_3 from the melt superior to α-Al_2O_3 thanks to lower interfacial energy between crystal and liquid [19,20]. The phase formation is known to be related to the melting of in-flight spray particles. The improvement of melting degree contributes the content of γ-Al_2O_3 [21]. From Fig. 6, it is evident that the relative intensity of γ-Al_2O_3 in the composite coating is higher than pure alumina coating. This may be resulted from the improved heating of particle contributed by addition of Al on the surface. On the other hand, from Fig. 6, it also can be seen that the metal Al phase clearly appears in Al_2O_3–Al feedstock particles, but is hardly found in the surface of corresponding composite coating. This

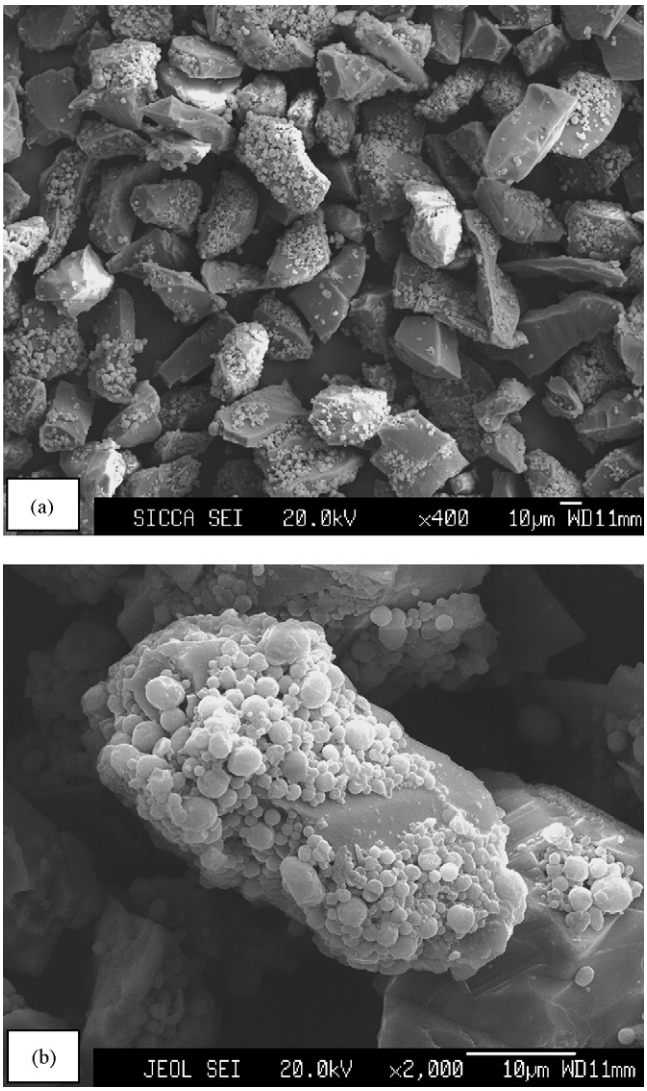

Fig. 3. SEM micrographs of Al_2O_3–Al composite powders.

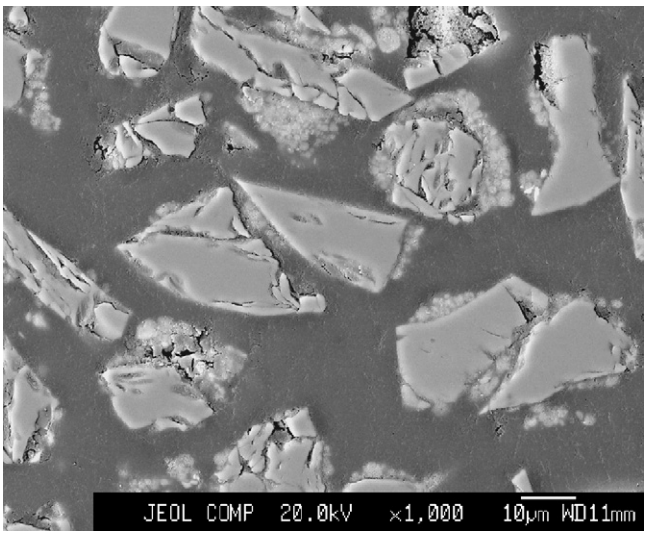

Fig. 4. SEM analysis of internal morphology of Al_2O_3–Al composite powders.

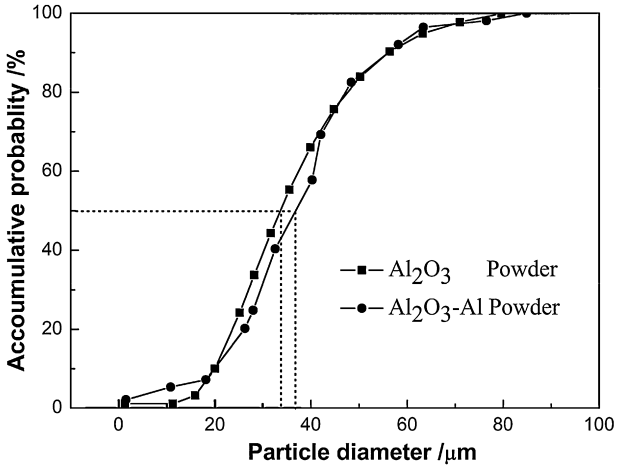

Fig. 5. Particle size distribution of both feedstock powders measured by a laser scattering method.

difference may arise due to the limitation of XRD technique for characterizing too low content of certain phase. In order to further investigate the existence and distribution of Al phase within Al_2O_3 matrix, the WDS element analysis of composite coating was performed, which will be described in following section.

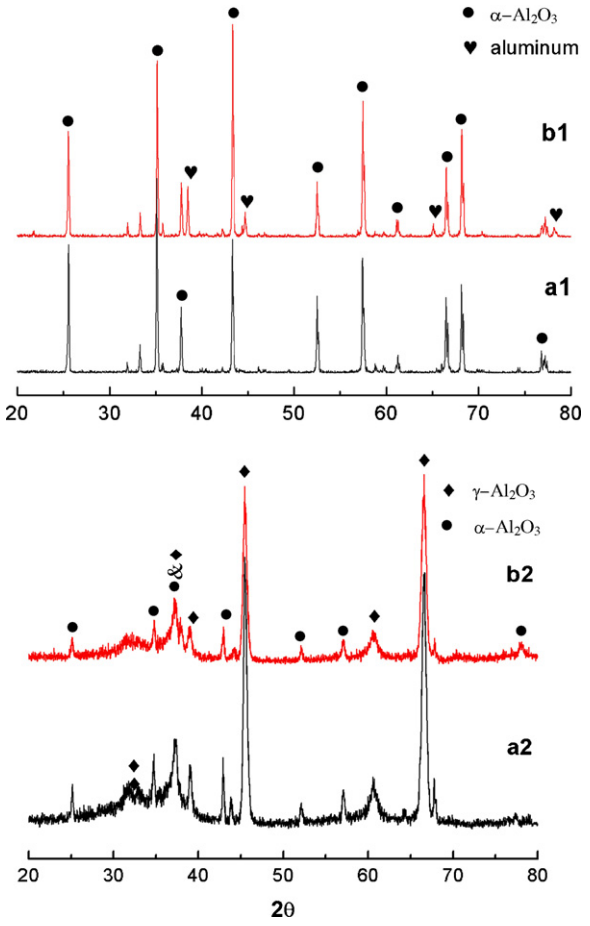

Fig. 6. X-ray diffraction patterns of the powders and as-sprayed coatings: (a1) Al_2O_3 powder; (a2) Al_2O_3 coating; (b1) Al_2O_3–Al powder and (b2) Al_2O_3–Al coating.

3.2. Microstructure of coatings

Fig. 7 shows the optical micrographs of individual and multiple droplets impacted on the unheated quartz substrate. It can be clearly seen that the impacted Al_2O_3 droplets exhibit a highly fragmented and splashing morphology with projections arising from the periphery. In comparison, the composite specimen presents relatively intact disk-like shape morphology with limited splashing, indicating a rather good particle flattening [22] and high deposition efficiency [23]. As shown in Table 2, the deposition efficiency of Al_2O_3–Al composite coating (49%) increased by about 30% compared with that of Al_2O_3 coating (37%). It is well known that upon impingement onto the cold substrate surface, the droplets lose their kinetic and thermal energies and thus experience ultrarapid solidification and concurrent high strain-rate deformation. It has also been pointed out that during spraying the ductile metallic particles such as aluminum can retain their plasticity for a sufficient time and generally conform to the local geometry of the surface [24]. On the other hand, a large amount of experimental and numerical works with respect to the droplet–substrate interactions and interfacial heat transfer have been carried out [25–30]. It is suggested that the droplet spreading and splashing are sensitive to numerous factors including the evaporation of adsorbed gases on substrate surface [25,26], molten state (in-flight characteristics) of droplet prior to impact [27], initiation or localized solidification due to weak and uniform thermal conduction between impacted droplet and substrate [28] and substrate properties (i.e., materials, surface roughness and temperature) [27,29,30]. Herein, the improvement of droplet splashing can be explained in terms of the Al addition for its well ductility and thermal conductivity, though the origin of these impinging droplet morphology changes is not clear at this time requiring more experimental and theoretical analysis.

The microstructural investigation of Al_2O_3 and Al_2O_3–Al composite coatings is shown in Figs. 8–10. Fig. 8 illustrates the cross-sectional morphologies of both coatings. It shows that the composite coating possesses homogeneously dispersed porosity and pores indicated by the black area in the microstructure are small with a few exceptions, besides, no macro-cracking is evident. However, in case of the Al_2O_3 coating, higher porosity with some big distinguished volumetric pores is observed (Fig. 8a), which are confirmed by the image analysis results that the porosities of Al_2O_3 and Al_2O_3–Al composite coatings are 8.3% and 6.4%, respectively (Table 2). Since it is not very distinguished and compellent to validate the existence of Al phase only by composition contrast from backscattered electron micron micrographs (Fig. 8b), the elemental analysis of WDS was performed to examine the distribution of Al phase within composite coating. Fig. 9 clearly demonstrates the content distribution of each element on the matrix map. Areas with very high content of Al and little O elements, or with little content of both two elements, are considered to be Al phase and cracks or pores, respectively. Accordingly, the positions of pores or micro-cracks are identifiable and the co-sprayed fully melted Al particles are deemed to be dispersed in the boundaries

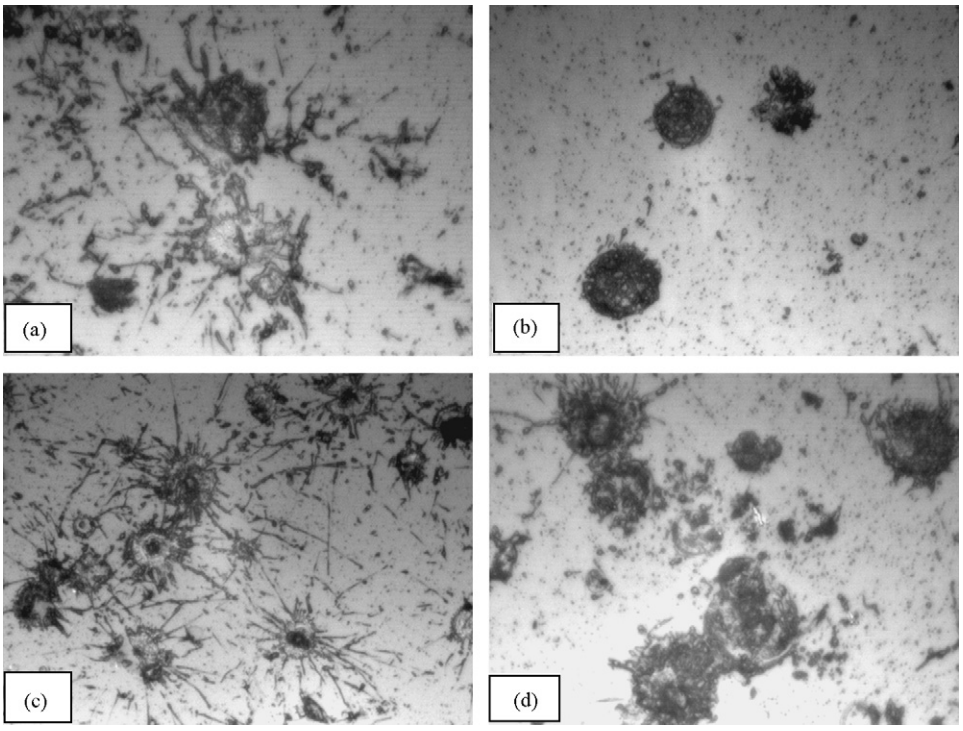

Fig. 7. Optical micrographs of individual and multiple droplets impacted on unheated quartz glass substrate: (a, c) Al_2O_3 and (b, d) Al_2O_3–Al specimens (Magnifications, 200×).

between Al_2O_3 phase and pores or micro-cracks, as well as in the splat border (see Fig. 8b and Fig. 9). In addition, it seems that the Al phase did not uniformly distribute along the all lamellar interface and the Al inclusions in the coating were relatively rather thick than that is expected from its composition of 5% and cladding feature on Al_2O_3. This can be understood that the melted Al on the Al_2O_3 surface may partially aggregate and separate with Al_2O_3 center owing to de-bonding of composite powders during in-flight for their different density and the evaporation of organic binder.

It is well known that in thermal spray the deposit is built up by successive impingement of the liquid or partially melted droplets onto substrates. The flattening and spreading of the impacting droplets, the 'brick' for the build up of the deposit, will ultimately determine the microstructure and properties of the deposit [31–33]. Good spreading and deformation of impacted droplet will lead to dense microstructure and developed inter-bonding between splats due to more contact points [16,34,35]. This is consistent with the comparison of fractured morphologies of coatings, as shown in Fig. 10 that compared with Al_2O_3 coating, the Al/Al_2O_3 composite coating possesses more distinct lamellar microstructure and improved splat interface, which is mainly attributed to its improved spreading and limited splashing (Fig. 7b, d).

Table 2
Porosity, deposition efficiency and thermal diffusivity of plasma-sprayed Al_2O_3 and Al_2O_3–Al composite samples

Samples	Porosity (%)	Deposition efficiency (%)	Thermal diffusivity at 200 °C ($\times 10^{-3}$ m^2/s)
Al_2O_3 coating	8.3	37	10.4
Al_2O_3–Al composite coating	6.4	49	13.3

3.3. Mechanical properties

Table 3 exhibits mechanical properties of Al_2O_3 and Al_2O_3–Al composite coatings. It can be known from Table 3 that the Vickers hardness of Al_2O_3–Al composite coating is around 845 $Hv_{0.2}$, which is slightly lower than that of the Al_2O_3 coating (870 $Hv_{0.2}$). However, increase in fracture toughness of composite coating compared with Al_2O_3 coating is up to 20%. It is well known that the Al_2O_3 ceramic is hard and brittle phase. Stress concentration and fine cracks easily form in the hard and brittle Al_2O_3 ceramic when the composite coating sustains impact and stress [10]. Metal Al, having excellent toughness, can restrain cracks expanding in virtue of stress releasing. To a certain extent, the multiphase metal Al and

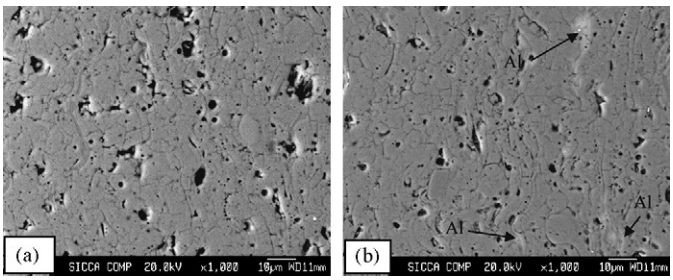

Fig. 8. Cross-sectional morphologies of the as-sprayed (a) Al_2O_3 and (b) Al_2O_3–Al composite coatings.

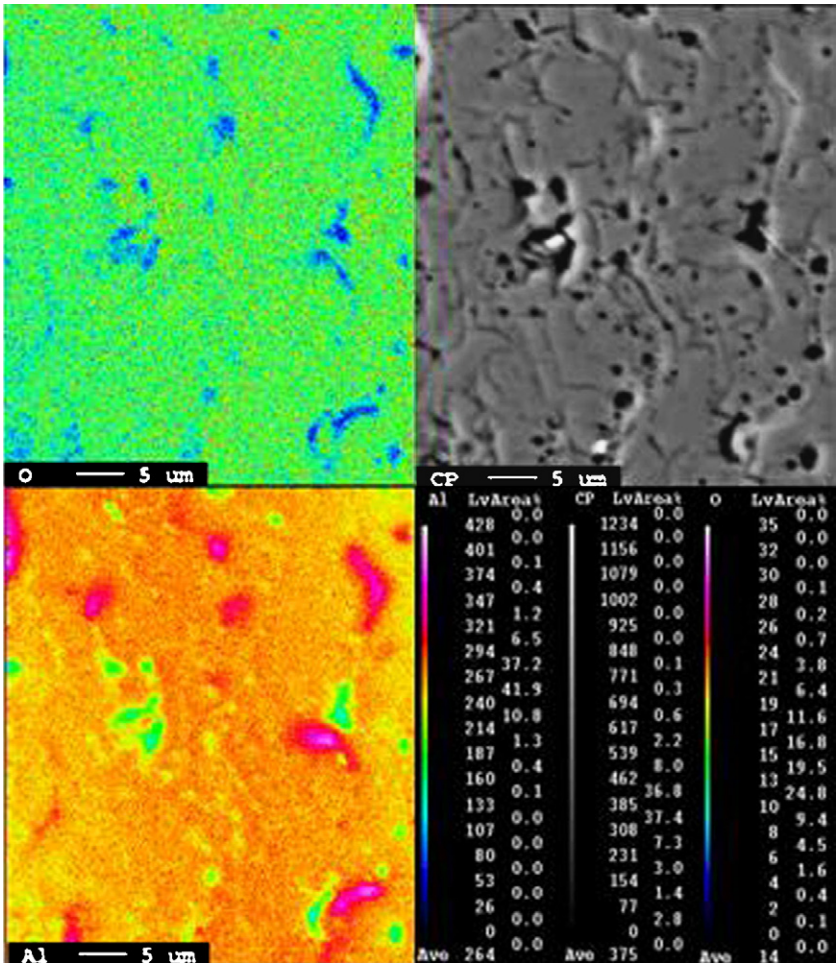

Fig. 9. SEM and WDS analysis of the cross-section of Al_2O_3–Al composite coatings.

Al_2O_3 ceramic coexistence can decrease the brittleness and improve the toughness of the Al_2O_3–Al composite coating.

It also can be seen that the adhesion and bending strength of the Al_2O_3–Al composite coating are 28.8 and 172 MPa, while that of Al_2O_3 coating are 22.6 and 147 MPa. The results obtained showed that the adhesion and bending strength of the composite coating, compared to Al_2O_3 coating increased by about 27% and 17%, respectively. It is generally accepted that in thermal spray deposit, there is limited real contact between the rapidly solidifying splats and the actual area of contact has been estimated at only around 20%, resulting in weak interface between splats [20,36]. A recent study on the lamellar bonding of plasma-sprayed Al_2O_3 coating suggested that the coating strength shows high dependence on the inter-bonding between the flattened droplets [37]. Concerning the nature of inter-bonding between flattened droplets, several studies have been carried out and a probable model advanced by Mcpherson [7] has been approved to a great extent that the inter-bonding is determined by a great deal of small distributed contact points between two solid surfaces. So, based on this model the cohesion between splats within Al_2O_3–Al composite coating is reasonably developed due to more contact points between well

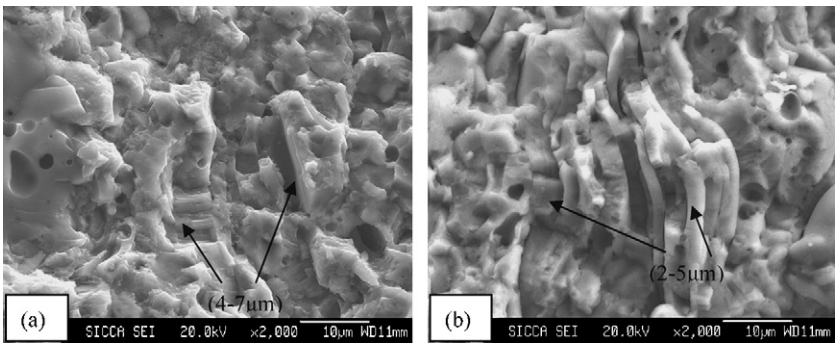

Fig. 10. SEM image of fractured morphologies of as-sprayed (a) Al_2O_3 coating and (b) Al_2O_3–Al composite coatings.

Table 3
Mechanical properties of Al_2O_3 and Al_2O_3–Al composite coatings

Samples	Microhardness ($Hv_{0.2}$)	Fracture toughness (MPa $m^{1/2}$)	Bending strength (MPa)	Adhesion strength (MPa)
Al_2O_3 coating	870 ± 60	2.7 ± 0.2	147.0 ± 9.2	22.6 ± 2.8
Al_2O_3–Al coating	845 ± 72	3.3 ± 0.3	172.0 ± 11.0	28.8 ± 3.2

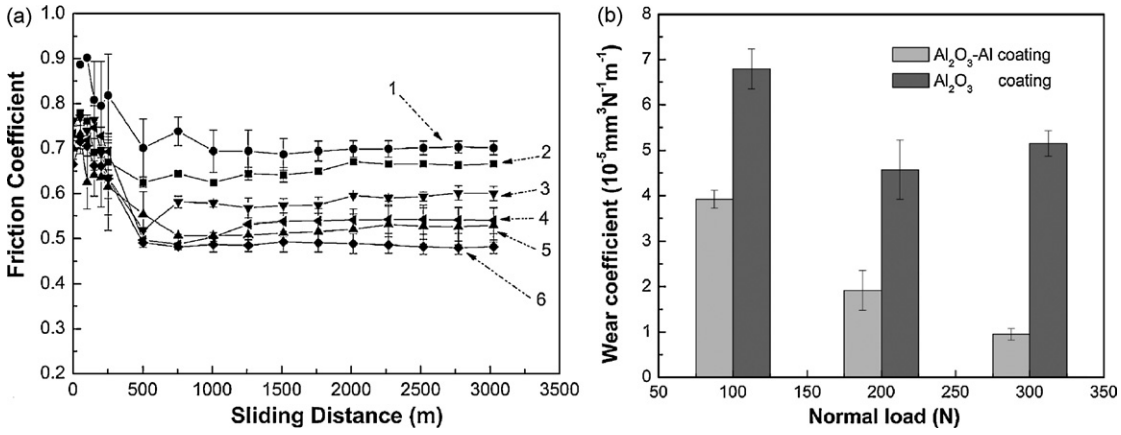

Fig. 11. Friction coefficient (a) and wear rate (b) of Al_2O_3 and Al_2O_3–Al composite coatings against stainless steel by block-on-ring configuration (1, 3, 5 and 2, 4, 6 in (a), respectively, represent the friction coefficient of Al_2O_3 and Al_2O_3–Al composite coatings under 100, 200, and 300 N and velocity of 0.84 m/s for 1 h duration).

flattening splats, as shown in Fig. 10, which may account for the better strength of Al_2O_3–Al composite coating superior to that of Al_2O_3 coating.

3.4. Wear resistance

Fig. 11 shows the friction coefficient and wear rate of Al_2O_3 and Al_2O_3–Al composite coatings against stainless steel as a function of different load using block-on ring arrangement. From Fig. 11, the Al_2O_3–Al composite coating possesses lower friction coefficient and wear rate than that of Al_2O_3 coating under the same conditions. The experimental results indicate that compared with Al_2O_3 coating, the composite coating exhibits better wear resistance. Numerous works have been carried out to realize the high dependence of wear resistance of plasma-sprayed coatings on its mechanical properties such as hardness, toughness and adhesion strength [38,39]. Despite the fact that pure Al_2O_3 coating has higher hardness, it is brittle phase in which macro-cracks easily come into being and expand under higher loads. In addition, tribological heat produced by friction during testing is difficult to diffuse and often concentrates on the real contact area of friction pairs, raising the temperature of the coating quickly and accelerating the wear of the ceramic coating. However, metal Al in the composite coating is an excellent conductor of heat, so the temperature of the composite coating remains relatively low even when the load rises to 300 N (see Fig. 12). Thus, the superior wear resistance of Al_2O_3–Al composite coating to that of Al_2O_3 coating can be attributed to its improved toughness, strength (Table 3) and thermal diffusivity (Table 2).

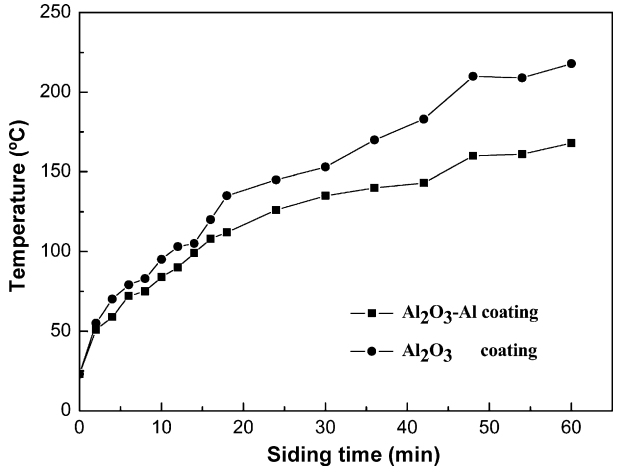

Fig. 12. The measured temperature characterizing tribological heat concentrated on the real contact of friction pairs under the load of 300 N using a block-on-ring configuration.

4. Conclusions

Al_2O_3 and Al_2O_3–Al composite coatings were deposited by plasma spraying. The Al additive effects and the correlation between coating microstructure, mechanical properties and wear resistance were investigated. The following points were found:

1. The addition of Al on Al_2O_3 particle surface is beneficial to decrease the splashing extent of the Al/Al_2O_3 composite droplet and increases its deposition efficiency. And the dense microstructure and developed inter-splat contact can be obtained for the Al/Al_2O_3 composite coating.
2. The Al_2O_3–Al composite coating possesses homogeneously dispersed pores and the co-sprayed Al particles are considered to be distributed in the splat boundary. Compared

with Al_2O_3 coating, the composite coating shows slightly lower hardness, whereas the coexistence of metal Al phase and Al_2O_3 ceramic phase effectively improves the toughness and strength of the coating.

3. The wear resistance of Al_2O_3–Al composite coating is superior to that of the Al_2O_3 coating under the same conditions using block-on-ring configuration. The improvement in anti-wear property of the composite coating can be attributed to its developed toughness, strength and thermal diffusivity, contributing to alleviate the concentration of tribological heat on real contact of friction pairs.

Acknowledgements

The authors wish to express their thanks to Ms. Zhenglan Lu and Weijun Qian for mechanical test and SEM analysis, and Dr. Xuanyong Liu and Youtao Xie for their constructive proposals and effective discussions during performing the present study.

References

[1] R. Westergard, L.C. Erickson, N. Axen, H.M. Hawthorne, S. Hogmark, The erosion and abrasion characteristics of alumina coatings plasma sprayed under different spraying conditions, Tribol. Int. 31 (1998) 271–279.

[2] W. Haessler, R. Thielsch, N. Mattern, Structure and electrical properties of PZT thick films produced by plasma spraying, Mater. Lett. 24 (1995) 387–391.

[3] J.F. Li, J.Q. Huang, S.H. Tan, Z.M. Cheng, C.X. Ding, Tribological properties of silicon carbide under water-lubricated sliding, Wear 218 (1998) 167–171.

[4] H.M. Hawthorne, L.C. Erickson, D. Ross, H. Tai, T. Troczynski, The microstructure dependence of wear and indentation of some plasma-sprayed alumina coatings, Wear 203–204 (1997) 709–714.

[5] K. Ramachandran, V. Selvarajan, P.V. Ananthapadmanabhan, K.P. Sreekumar, Microstructure, adhesion, microhardness, abrasive wear resistance and electrical resistivity of the plasma sprayed alumina and alumina-titania coatings, Thin Solid Films 315 (1998) 144–152.

[6] C.J. Li, B. Sun, Effects of spray parameters on the microstructure and property of Al_2O_3 coatings sprayed by a low power plasma torch with a novel hollow cathode, Thin Solid Films 450 (2004) 282–289.

[7] R. Mcpherson, The relationship between the mechanism of formation, microstructure and properties of plasma-sprayed coatings, Thin Solid Films 83 (1981) 297–310.

[8] D.I. Pantelis, P. Psyllaki, N. Alexopoulos, Tribological behaviour of plasma-sprayed Al_2O_3 coatings under severe wear conditions, Wear 237 (2000) 197–204.

[9] Y.C. Dong, D.R. Yan, J.N. He, X.Z. Li, W.R. Feng, H. Liu, Studies on composite coatings prepared by plasma spraying Fe_2O_3–Al self-reaction composite powders, Surf. Coat. Technol. 179 (2004) 223–228.

[10] S.O. Chwa, D. Klein, F.L. Toma, G. Bertrand, H.L. Liao, C. Coddet, A. Ohmori, Microstructure and mechanical properties of plasma sprayed nanostructured TiO_2–Al composite coatings, Surf. Coat. Technol. 194 (2005) 215–224.

[11] X.H. Lin, Y. Zeng, S.W. Lee, C.X. Ding, Characterization of alumina-3 wt.% titania coating prepared by plasma spraying of nanostructured powders, J. Eur. Ceram. Soc. 24 (2004) 627–634.

[12] Z.Y. Deng, T. Fukasawa, M. Ando, G.J. Zhang, T. Ohji, Microstructure and mechanical properties of porous alumina ceramics fabricated by the deposition of aluminum hydroxide, J. Am. Ceram. Soc. 84 (2001) 2638–2644.

[13] J.F. Li, H. Liao, B. Normand, C. Cordier, G. Manurin, J. Foct, C. Coddet, Uniform design method for optimization of process parameters of plasma sprayed TiN coatings, Surf. Coat. Technol. 176 (2003) 1–13.

[14] S. Ying, Advanced Ceramics and Their Applications, Beijing Press of Science and Technology, Beijing, China, 1990 (in Chinese).

[15] S. Leigh, A. Lin, C.C. Berndt, Elastic response of thermal spray deposits under indentation tests, J. Am. Ceram. Soc. 80 (1997) 2093–2099.

[16] C.J. Li, W.Z. Wang, Y. He, Dependency of fracture of toughness of plasma-sprayed Al_2O_3 coatings on the microstructure, J. Therm. Spray Technol. 13 (2004) 425–431.

[17] C.J. Li, W.Z. Wang, Y. He, Measurement of fracture toughness of plasma-sprayed Al_2O_3 coatings using a tapered doubled beam method, J. Am. Ceram. Soc. 86 (2003) 1437–1439.

[18] P. Ostojic, R. Mepherson, Indentation toughness testing of plasma sprayed coatings, Mater. Forum 10 (1987) 247–254.

[19] R. Mcpherson, On the formation of thermally sprayed alumina coatings, J. Mater. Sci. 15 (1980) 3141–3149.

[20] R. Mcpherson, A review of microstructure and properties of plasma sprayed ceramic coatings, Surf. Coat. Technol. 39/40 (1989) 173–181.

[21] Y. Gao, X.L. Xu, Z.J. Yan, G. Xin, High hardness alumina coatings prepared by low power plasma spraying, Surf. Coat. Technol. 154 (2002) 189–193.

[22] M. Fukumoto, P. Fauchais, A. Grimaud, Influence of substrate roughness and temperature on the adhesion/cohesion of alumina coatings, Surf. Coat. Technol. 81 (1996) 275–286.

[23] A. Kulkarni, Z. Wang, T. Nakamura, Comprehensive microstructure characterization and predictive property modeling of plasma-sprayed zirconia coatings, Acta Mater. 51 (2003) 2457–2475.

[24] S. Safai, H. Herman, Microstructural investigation of plasma-sprayed aluminum coatings, Thin Solid Films 45 (1977) 295–307.

[25] X.Y. Jiang, Y.P. Wan, H. Herman, S. Sampath, Role of condensates and adsorbates on substrate surface on fragmentation of impinging molten droplets during thermal spray, Thin Solid Films 385 (2001) 132–141.

[26] C.J. Li, J.L. Li, Evaporated-gas-induced splashing model for splat formation during plasma spraying, Surf. Coat. Technol. 184 (2004) 13–23.

[27] R.C. Dykhuizen, Review of impact and solidification of molten thermal spray droplets, J. Therm. Spray Technol. 3 (1994) 351–361.

[28] A. Vardelle, N.J. Themelis, M. Vardelle, B. Dussoubs, P. Fauchais, Transport and chemical rate phenomena in plasma sprays, High Temp. Mater. Processes 3 (1997) 295–314.

[29] M.F. Morks, Y. Tsunekawa, M. Okumiya, M.A. Shoeib, Splat morphology and microstructure of plasma sprayed cast iron with different substrate temperature, J. Therm. Spray Technol. 11 (2002) 262–269.

[30] A. Abedini, A. Pourmousa, S. Chandra, J. Mostaghimi, Effect of substrate temperature on the properties of coatings and splats deposited by wire arc spraying, Surf. Coat. Technol. 201 (2006) 3350–3358.

[31] X. Jiang, J. Matejicek, S. Sampath, Substrate temperature effects on the splat formation, microstructure development and properties of plasma sprayed coatings part II: case study for molybdenum, Mater. Sci. Eng. A 272 (1999) 189–198.

[32] J.E. Blendell, R.L. Coble, Measurement of stress due to thermal expansion anisotropy in Al_2O_3, J. Am. Ceram. Soc. 65 (1982) 174–177.

[33] A. Ohmori, C.J. Li, Quantitative characterization of the structure of plasma sprayed Al_2O_3 coating by using copper electroplating, Thin Solid Films 201 (1991) 241–252.

[34] S. Sampath, X. Jiang, Splat formation and microstructure development during plasma spraying: deposition temperature effects, Mater. Sci. Eng. A 304–306 (2001) 144–150.

[35] C.J. Li, A. Ohmori, Relationship between the structure and properties of thermally sprayed coatings, J. Therm. Spray Technol. 11 (2002) 365–374.

[36] R.S. Lima, A. Kucuk, C.C. Berndt, Evaluation of microhardness and elastic modulus of thermally sprayed nanostructured zirconia coatings, Surf. Coat. Technol. 135 (2001) 166–172.

[37] C.J. Li, B. Sun, Microstrcuture and property of Al_2O_3 coating micro-plasma-sprayed using a novel hollow cathode torch, Mater. Lett. 58 (2003) 179–183.

[38] B. Normand, V. Fervel, C. Coddet, V. Nikitine, Tribological properties of plasma sprayed alumina-titania coating: role and control of the microstructure, Surf. Coat. Technol. 123 (2000) 278–287.

[39] L.C. Erickson, H.M. Hawthome, T. Troczynski, Correlations between microstructural parameters, micromechanical properties and wear resistance of plasma sprayed ceramic coating, Wear 250 (2001) 569–575.